

# All-gel Proton-conducting Batteries with BiOCl and VOSO<sub>4</sub> as Active Materials

Prathap Iyapazham Vaigunda Suba,<sup>[a]</sup> Muhammad Shoaib,<sup>[a]</sup> Oanh Hoang Nguyen,<sup>[a]</sup> Kunal Karan,<sup>[b]</sup> Stephen R. Larter,<sup>[c]</sup> and Venkataraman Thangadurai\*<sup>[a]</sup>

Flexible, scalable, and low-cost energy storage solutions are required for the widespread use of renewable energy and the mitigation of climate change. State-of-the-art lithium-ion batteries provide high specific energy density; however, designing a safe and cost-effective grid-scale lithium-ion battery is still a major challenge. Redox flow batteries are scalable due to their ability to decouple power and energy; however, the commercial applications of these batteries are limited because of expensive ion-selective membranes. In this paper, we report a modified

battery design approach in which Bi/BiOCl and V<sup>4+</sup>/V<sup>5+</sup> reaction-based redox couples are utilized while employing a gel-based architecture. We show, for the first time, that Bi/BiOCl conversion reaction based redox couple can reversibly work against traditional vanadium-based redox pair in an aqueous electrolyte. Redox active materials in this cell design are in the gel form, and a traditional membrane or a separator is not required. This proof-of-concept battery delivers 0.9 V with a volumetric energy density of 22.14 Wh/L.

## Introduction

Development of new energy storage technologies, that are scalable and cost effective, has become a critical challenge in this century to help alleviate the climate change issue.<sup>[1]</sup> Cost of energy from renewable sources is continuously decreasing, however, their application is still not mainstream in many communities due to their intermittent nature and requirement of an energy storage medium.<sup>[2]</sup> Lithium-ion batteries are excellent in terms of energy density and efficiency; however, this battery technology struggles in terms of cost, safety, and scalability for large scale applications.<sup>[3]</sup> Redox flow batteries, on the other hand, are scalable but still expensive due to the inclusion of ion-selective membranes and the requirement of large electrolyte tanks and pumping of solutions.<sup>[4]</sup> Redox flow batteries utilize electro-active materials dissolved in electrolytes that lay down another requirement for electro-active materials being soluble in solutions, and it also limits the operating

temperature of these batteries. The volumetric energy density of a redox flow battery depends on the solubility of the active materials. The commercialized vanadium-based redox flow batteries have been reported to have volumetric energy densities as high as 36 Wh/L and organic electro-active materials like quinones have been developed, which shows volumetric energy density up to 50 Wh/L.<sup>[5]</sup>

To mitigate some of the challenges of current battery technologies, battery architecture using non-conventional methodologies has been widely studied. Membrane-free redox flow batteries, semi-solid flow batteries, and biphasic batteries have been recently demonstrated.<sup>[6]</sup> Skyllas-Kazacos et al., demonstrated gel-based vanadium batteries which used Nafion membrane as separator.<sup>[7]</sup> Gautam et al., demonstrated polymerization gel type electrolytes for batteries which involves either batteries with membranes or without membranes.<sup>[8]</sup> Aqueous Li-ion batteries using water-in-salt electrolytes or using additives are also being studied.<sup>[9]</sup> All these approaches are aimed to achieve higher energy density of batteries and despite their success, energy density of these batteries is limited by the solubility limits of electro-active materials or coating density. We report, for the first time, a new approach of dispersing (or dissolving) the electro-active materials in suitable electrolytes and then forming a gel by the addition of fumed silica as a gelling agent. By gel formation, electroactive materials will stay dispersed in a three-dimensional gel structure without any possibility of agglomeration or settling down. The use of conventional separators (as in lithium-ion batteries) or membranes (as in redox flow batteries) is alleviated in this novel battery design by adding a sandwich electrolyte gel layer between the electro-active gels. The selection of materials in this sandwich layer is made in such a way that it bars the electronic conduction between the electro-active (cathode and anode) gels, but mobile ions can permeate through this layer. This radical new design can offer low cost, flexible design, and

[a] P. Iyapazham Vaigunda Suba, Dr. M. Shoaib, O. Hoang Nguyen, Prof. V. Thangadurai  
Department of Chemistry  
University of Calgary  
Calgary, Alberta T2N 1N4 (Canada)  
E-mail: vthangad@ucalgary.ca

[b] Prof. K. Karan  
Department of Chemical and Petroleum Engineering  
University of Calgary  
Calgary, Alberta T2N 1N4 (Canada)

[c] Prof. S. R. Larter  
Department of Earth, Energy, and Environment  
University of Calgary  
Calgary, Alberta, T2N 1N4 (Canada)

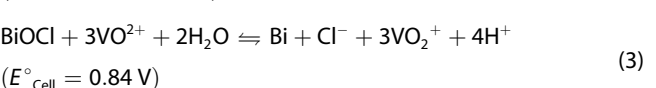
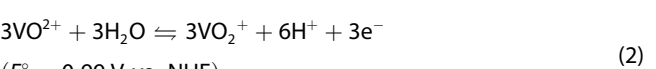
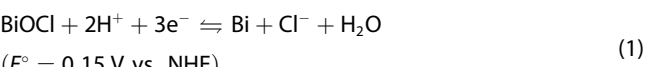
© 2023 The Authors. *Batteries & Supercaps* published by Wiley-VCH GmbH. This is an open access article under the terms of the Creative Commons Attribution Non-Commercial NoDerivs License, which permits use and distribution in any medium, provided the original work is properly cited, the use is non-commercial and no modifications or adaptations are made.

new possibilities of electrode materials with very high volumetric energy density.

Vanadium is a widely studied electro-active material in large-scale redox flow batteries. Typically, vanadium redox flow batteries operate at  $\text{H}_2\text{SO}_4$  concentrations greater than 1 M ( $\text{pH}=0$ ).  $\text{BiOCl}$  has been recently studied as conversion-type electrodes in aqueous batteries with  $\text{AlCl}_3$  as electrolyte in  $\text{pH}>2.73$ .<sup>[10]</sup>  $\text{BiOCl}$  is also used in desalination electrodes as chloride storage medium by utilizing the conversion type reaction between  $\text{Bi}/\text{BiOCl}$ .<sup>[11]</sup> Nam et al. studied the stability of  $\text{BiOCl}$  in acid environment when chloride ions are present in the solution.<sup>[12]</sup> In our proof-of-the-concept all-gel battery, we have used  $\text{VOSO}_4$  as the positive electrode material and  $\text{BiOCl}$  as the negative electrode material. Inclusion of this new redox pair gives a discharge voltage of 0.9 V in protic conditions. Graphite felt is used as current collector in both anode and cathode sides of the battery. Electrochemical experimental measurements show that this battery can deliver a high reversible capacity of 22.14 Wh/L, based on volume of both anode and cathode gel. The electrochemical reaction mechanism of this new redox pair was investigated by using electrochemical and material characterization techniques. This novel design will open new opportunities for low-cost batteries owing to its simple and flexible design and ability to use variety of different electro-active materials irrespective of their solubility in the electrolytes.

## Results and Discussion

Expected voltage of the cells were calculated by assembling the half cells, using individual electrode materials in gel form in 1 M  $\text{HCl}+1 \text{ M H}_2\text{SO}_4$  with 15 wt% fumed silica and measuring the cyclic voltammograms (CV) with Pt counter electrode and  $\text{Ag}/\text{AgCl}$  (sat. KCl) as reference electrode.  $\text{BiOCl}$  electrode provides distinct and high intensity peaks compared to that of  $\text{V}^{4+}/\text{V}^{5+}$  at the same scan despite its conversion reaction-based mechanism. Thermodynamic standard reduction potential values for  $\text{BiOCl}/\text{Bi}$  and  $\text{V}^{4+}/\text{V}^{5+}$  redox reaction are 0.15 V and 0.99 V, respectively, as shown along the reactions (1) and (2). In theory this redox couple would provide a theoretical open circuit voltage of 0.84 V. The proposed half cells and full cell reactions are:



The obtained cell potential based on the cyclic voltammetry is 1.01 V, calculated from the difference of  $E_{1/2}$  from  $\text{VOSO}_4$  and  $\text{BiOCl}$  [0.90–(−0.11)=1.01] as shown in Figure 1(a). The ionic conductivity of the silica gel in 1 M  $\text{HCl}+1 \text{ M H}_2\text{SO}_4$  was measured at different weight percentages of fumed silica using a custom-made two electrode configuration cell with Pt electrode.  $\text{SiO}_2$  (fumed silica) was used as a gel former that is known as semiconductor, its utilization in this battery may reduce the conductivity in the electrodes and ionic mobility in the electrolyte. However, EIS measurements of the electrolyte solutions with different concentrations of fumed silica show minor changes in the solution resistance. Figure 1(b) shows the Nyquist plots of electrolytes at different concentrations of fumed silica. It was observed that electrolyte resistance increases from 1.64 ohm to 2.65 ohm only, by increasing silica concentration up to 25%, as shown in Figure 1(b). The ionic conductivity of the 1 M  $\text{HCl}+1 \text{ M H}_2\text{SO}_4$  with 0% fumed silica is  $\sigma=0.48 \text{ S/cm}$  (calculated using the expression  $\sigma=\text{cell constant}/\text{solution resistance}$ ). The ionic conductivity of gels with fumed silica wt/vol % content from 5%, 10%, 15%, 20%, and 25% ranges from 0.39 S/cm, 0.37 S/cm, 0.35 S/cm, 0.31 S/cm, and 0.29 S/cm. So, it can be safely assumed that making a viscous silica gel does not significantly impact the solution conductivity. Moreover, the ionic conductivity values of the gel with different fumed silica concentrations are within the range of ionic conductivity of electrolytes studied for vanadium redox flow batteries (0.17 to 0.44 S/cm).<sup>[13]</sup>

Wang et al. categorized electrochemical reactions into three tiers of reversibility: reversible, quasi-reversible, and irreversible depending on their behavior in CV measurements.<sup>[14]</sup> Based on the peak-to-peak separation values of  $\text{BiOCl}/\text{Bi}$  and  $\text{VO}_2^+/\text{VO}^{2+}$  systems, we conclude that  $\text{BiOCl}/\text{Bi}$  is quasi-reversible, and  $\text{VO}_2^+/\text{VO}^{2+}$  is irreversible, which agrees with previous literatures.<sup>[10,15]</sup> From the cyclic voltammetry data the Tafel plots for  $\text{VOSO}_4$  in

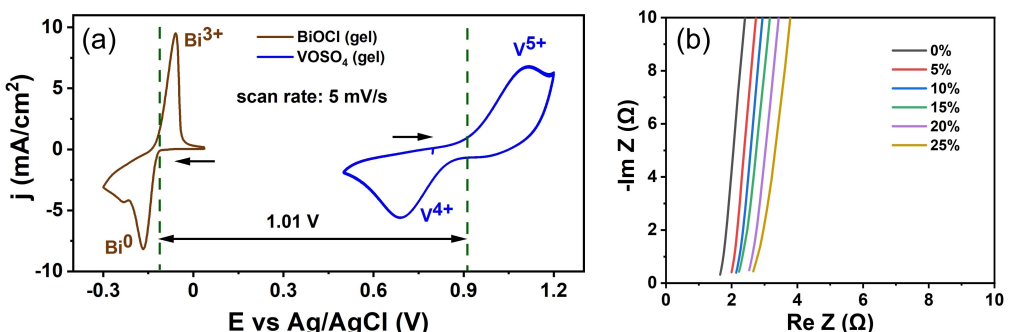


Figure 1. a) Cyclic voltammogram of  $\text{VOSO}_4$  and  $\text{BiOCl}$  in gel electrodes, b) EIS of 1 M  $\text{HCl}+1 \text{ M H}_2\text{SO}_4$  with varying percentages of fumed silica.

both the solution and gel form and for BiOCl in coated and gel form were plotted as shown in Figure 2(a and b). The Tafel slopes and exchange current density are tabulated in Table 1. The Tafel slopes for solution and gel for VOSO<sub>4</sub> and coated and gel for BiOCl are in close ranges. This shows that the mechanism of electrochemical reactions in the case of conventional electrode setup and the gel form remains the same. In the case of VOSO<sub>4</sub>, the exchange current density decreases in gel compared to solution form, which is reasonable as with gel the active area will decrease compared to solution. However, in the case of BiOCl in gel form the exchange current density increases to 0.697 mA/cm<sup>2</sup> from 0.334 mA/cm<sup>2</sup> of coated electrode form, which shows that the BiOCl in gel form has more active area compared to coated electrode form.

The full cell and half-cell performances were studied using galvanostatic charge/discharge experiments in different cell configurations to understand the electrochemical reaction mechanism. Initially to characterize the conversion reaction of BiOCl electrode, a full cell was assembled with VOSO<sub>4</sub> in gel form as positive electrode and BiOCl coated on graphite felt as negative electrode, a schematic diagram of this configuration is shown in Figure 3(a). The voltage profile of the charge discharge cycle is shown in Figure 3(b) in which a discharge potential of 0.96 V was obtained in the fifth cycle. The cell can retain a Coulombic efficiency of 94% for 100 cycles as shown in Figure 3(c).

To verify the electrochemical reaction mechanism of the BiOCl electrode, XRD measurements were performed for

**Table 1.** Tafel slope and exchange current density values for VOSO<sub>4</sub> and BiOCl.

Electrode type	Tafel slope [mV/decade]	Exchange current density [mA/cm <sup>2</sup> ]
1 M VOSO <sub>4</sub> solution	Oxidation – 95.7 Reduction – 80.0	1.768
VOSO <sub>4</sub> gel	Oxidation – 88.1 Reduction – 72.7	0.142
BiOCl coated on graphite felt	Oxidation – 22.9 Reduction – 191.4	0.334
BiOCl gel	Oxidation – 26.3 Reduction – 222.1	0.697

pristine electrode, at fully charged and discharged states. These XRD patterns are shown in Figure 4(a). These patterns show the signature XRD profile of tetragonal BiOCl phase with P4/nmm space group for the pristine electrode, confirmed by comparison with the Joint Committee on Powder Diffraction Standards (JCPDS) card 82-0485. While charging phase evolution takes place and the pattern representing the end of charge state can be indexed to a rhombohedral unit cell with R3m space group,

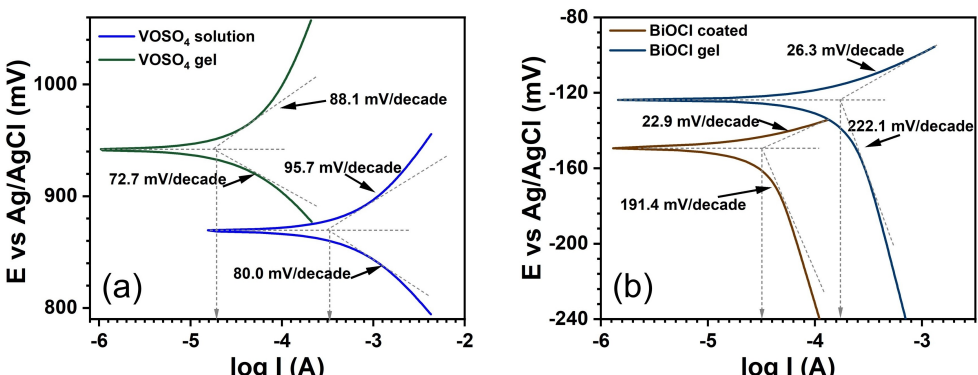


**Figure 2.** a) Tafel plot of VOSO<sub>4</sub> in solution and gel and b) Tafel plot of BiOCl for coated and gel electrode.

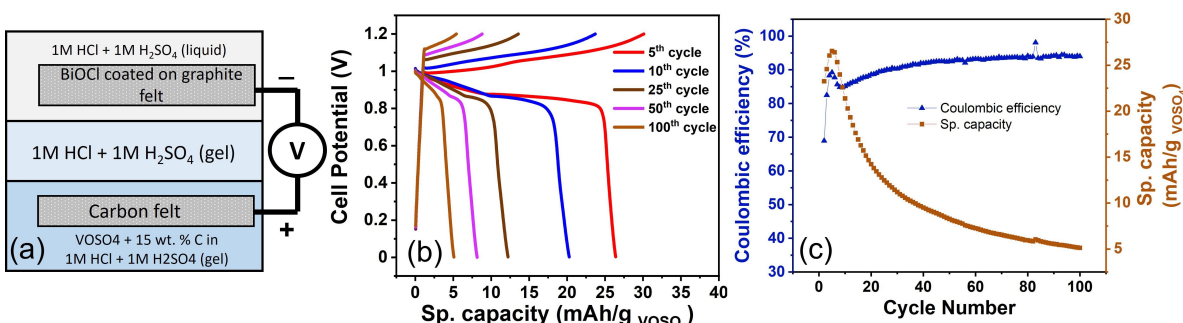


**Figure 3.** a) Schematic diagram of cell assembly with VOSO<sub>4</sub> in gel and BiOCl coated electrode, b) charge discharge voltage profiles and c) Coulombic efficiency along with the specific capacity based on mass of VOSO<sub>4</sub> in gel.

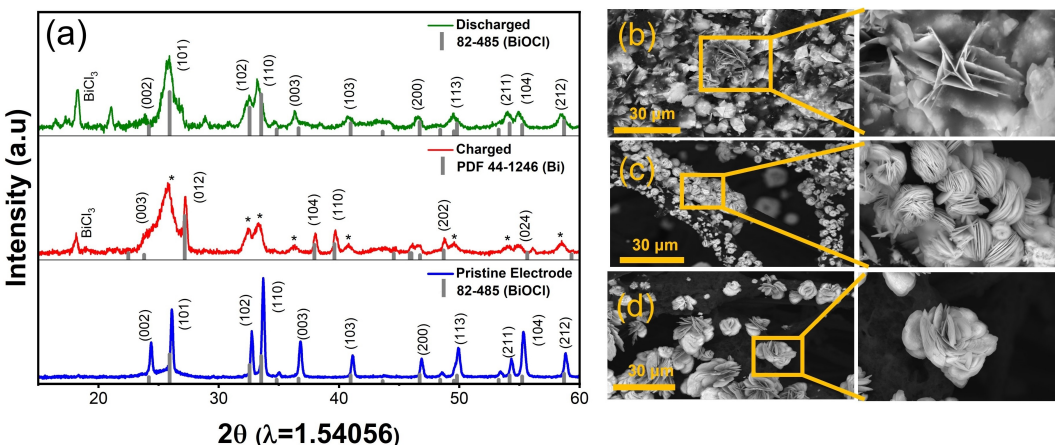


**Figure 4.** a) XRD patterns of pristine, charged and discharged BiOCl electrode and SEM images of b) BiOCl coated on graphite felt pristine electrode at c) charged state and d) discharged state.

JCPDS card 44-1246, indicating the formation of Bi metal. Peak intensity and sharpness noticeably decrease after the first charge, that can be ascribed to formation of nano dispersed phases as a result of conversion reaction. It is interesting to note that after the charge process, Bi metal phase peak appears, however BiOCl peaks do not disappear completely even though their intensity significantly drops, these residue peaks are marked with asterisks in Figure 4(a). During the discharge process Bi metal peaks disappear and BiOCl peaks reappear. It can be observed in XRD patterns that a small amount of  $\text{BiCl}_3$  is also formed during the electrochemical cycling.

The BiOCl electrodes morphology was studied using SEM as shown in Figure 4(b-d). The SEM image of the as-prepared BiOCl electrode coated on graphite felt is shown in Figure 4(b). In charged condition, as shown in Figure 4(c) (electrochemically converted to Bi) the morphology has changed from thin sheets to flower-petal-like sheets. The electrode in discharged condition as shown in Figure 4(d) (electrochemically converted back to BiOCl), the sheet like structure is retained with slight morphology change. These changes in morphology shows the reversible conversion between BiOCl to Bi.

Half-cells were assembled with gel type electrodes in three-electrode setup to study the electrochemical characteristics of individual electro-active gel electrodes. The three-electrode setup was assembled in a two-compartment cell with active material gel in one compartment, 1 M HCl + 1 M  $\text{H}_2\text{SO}_4$  solution in another compartment and separated by 15% silica gel in 1 M HCl + 1 M  $\text{H}_2\text{SO}_4$ . Graphite felt was used as current collectors for the gels, Pt as counter electrode and Ag/AgCl (sat. KCl) as reference electrode was inserted in the compartment with 1 M HCl + 1 M  $\text{H}_2\text{SO}_4$  solution. The gel electrodes were prepared in such a way that the capacity based on the active material is 1.25 mAh/ml of gel. The half-cell performance of  $\text{VOSO}_4$  gel is shown in Figure 5(a). The expected reactions in the half-cells are as follows: WE:  $\text{VO}^{2+} + \text{H}_2\text{O} \rightleftharpoons \text{VO}_2^+ + 2\text{H}^+ + \text{e}^-$ ; CE:  $2\text{H}^+ + 2\text{e}^- \rightarrow \text{H}_2$ . The  $\text{V}^{4+/5+}$  reactions plateau formed between 0.9 to 1.0 V vs. Ag/AgCl which is close to the value obtained from cyclic voltammetry studies. The cells showed 98% Coulombic

efficiency over 200 cycles and could retain a volumetric capacity of 266 mAh/l of  $\text{VOSO}_4$  gel as shown in Figure 5(b). The initial drop in capacity retention during the cycling of battery can be attributed to the loss of  $\text{V}^{4+/5+}$  ions from the gel due to crossover. For BiOCl electrode half-cell, the expected reactions are WE:  $\text{BiOCl} + 2\text{H}^+ + 3\text{e}^- \rightleftharpoons \text{Bi} + \text{Cl}^- + \text{H}_2\text{O}$ ; CE:  $2\text{H}_2\text{O} \rightarrow \text{O}_2 + 4\text{H}^+ + 4\text{e}^-$ . A typical half-cell plateau for the 10<sup>th</sup> cycle for BiOCl is shown in Figure 5(c) and the cyclic performance is shown in Figure 5(d). BiOCl in gel electrodes can retain the capacity for 20 cycles, after cycling beyond 20 cycles the overpotential increases and limits the capacity.

All-gel full cells were assembled with high and ultrahigh loading of electro-active materials. Cell geometry of the all-gel high loading cell is shown in Figure 6(a) and the electrochemical cycling performance of this cell is shown in Figure 6(b). Voltage profiles shown in Figure 6(b) during the charge and discharge process demonstrate distinct plateaus at around 0.9 V that is close to expected voltage, indicating that the expected BiOCl/Bi and  $\text{V}^{4+/5+}$  electrochemical reactions are taking place. Figure 6(c) shows the discharge capacity increased initially and started to decrease after 14 cycles, however the Coulombic efficiency is above 90% after 12<sup>th</sup> cycle.

To demonstrate the practical applications of the system, an ultra-high loading all-gel cell was assembled as shown in Figure 7(a), in which both the  $\text{VOSO}_4$  and BiOCl are prepared in silica gel with a cell capacity of 110 mAh. The battery was charged and discharged at C/20 and in the first cycle the battery showed a discharge capacity of 24.6 Ah/L and an average discharge voltage of 0.9 V, as shown in Figure 7(b) which converts to 22.14 Wh/L. The battery could demonstrate a Coulombic efficiency of above 90% as shown in Figure 7(c). However, further optimization studies are required in order to demonstrate the battery architecture for long cycle life. The demonstrated proof-of-concept battery design successfully shows that the capacity of active materials can go beyond their solubility limits in aqueous electrodes and insoluble materials can also be used as active materials without the need for coating of active materials.

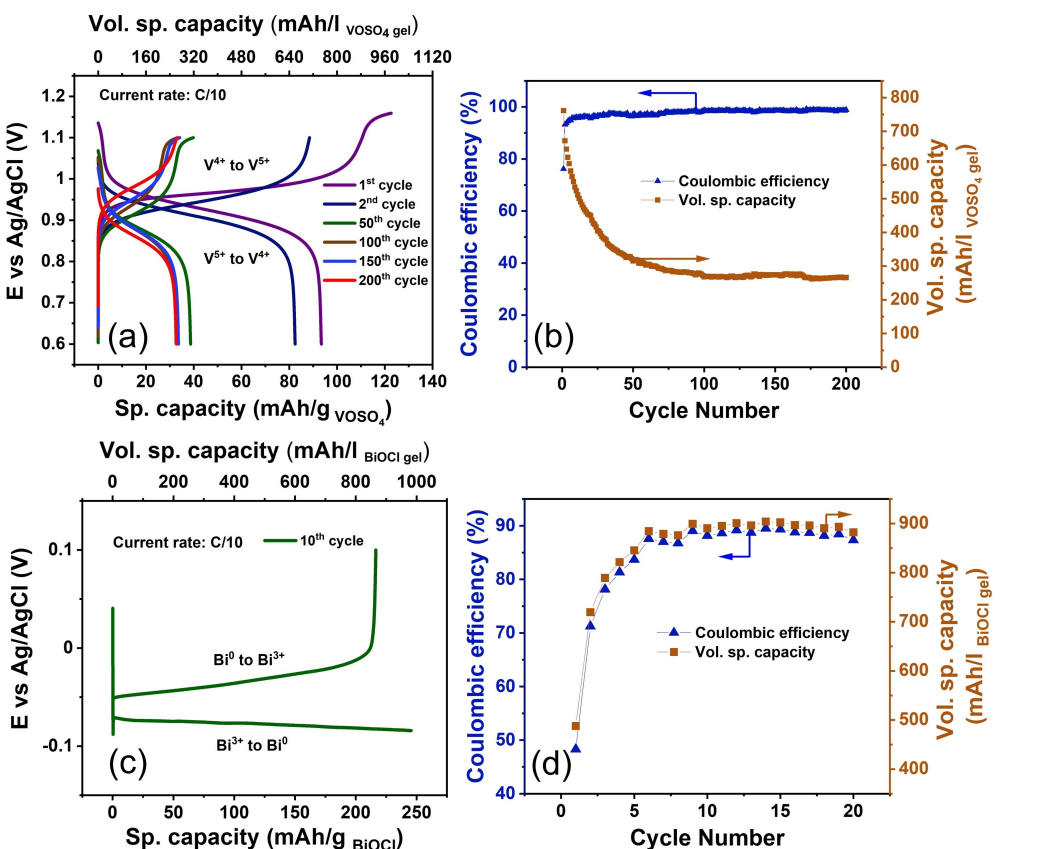


Figure 5. a) Half-cell capacity of VOSO<sub>4</sub> gel type cell, b) Coulombic efficiency along with volumetric capacity of VOSO<sub>4</sub> gel type cell, c) half-cell capacity of BiOCl gel type cell and d) Coulombic efficiency along with volumetric capacity of BiOCl gel type cell.

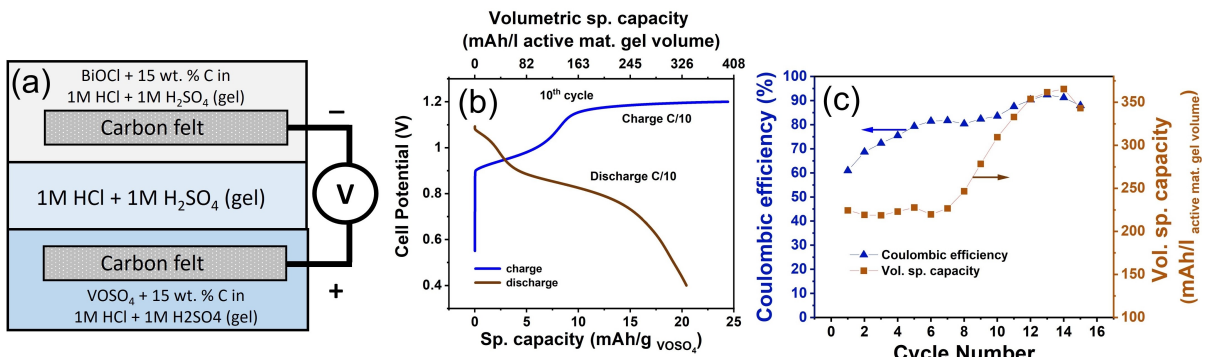
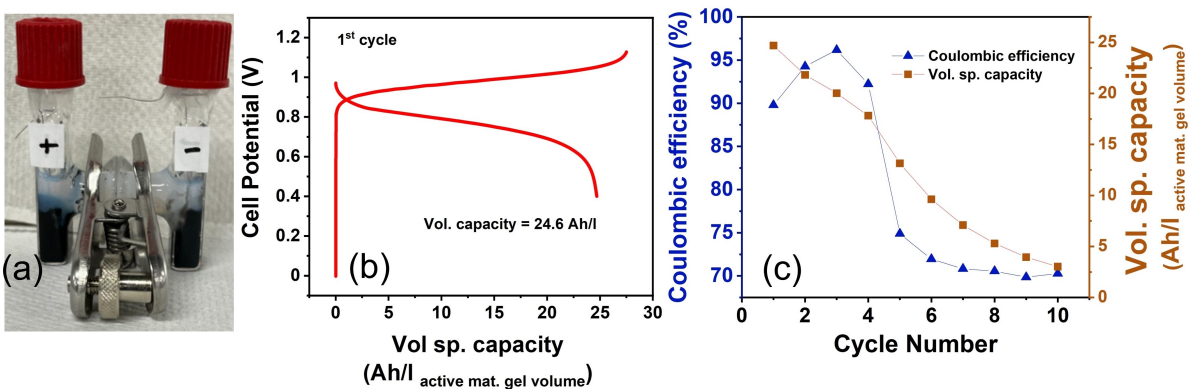


Figure 6. a) Schematic of the high loading cell setup, b) charge discharge voltage profile in the 10<sup>th</sup> cycle, and c) cycling performance and Coulombic efficiency in 15 initial cycles.

## Conclusions

We have demonstrated a proof-of-the-concept gel-based design of battery that can offer flexible design, high capacity, new choices of electrode materials and lower cost compared to current commercial batteries. EIS measurements show that resistance of gel does not significantly increase by adding up to 25 wt% of gel forming fumed silica. In this study we also explored a new combination of conversion type BiOCl/Bi electrode with V<sup>4+</sup>/V<sup>5+</sup> pair as active material. The electrochemical conversion reaction mechanism of BiOCl was con-

firmed by XRD measurements in our studies. The proof-of-the-concept system showed a volumetric energy density of 22.14 Wh/L. This new design and new electrode material will provide pathways for the design of next generation high energy density batteries that will fulfil the requirements of a niche battery market driven by cost and ease of manufacturing.



**Figure 7.** a) Photograph of the ultra-high loading cell setup, b) charge discharge voltage profile in the 1<sup>st</sup> cycle, and c) Coulombic efficiency and volumetric capacity in 10 cycles.

## Experimental Section

Vanadium oxide sulfate hydrate (Sigma Aldrich), fumed silica (Fisher Scientific), sulfuric acid, hydrochloric acid, super P conductive carbon (MTI corporation), Bismuth (III) oxychloride (Fisher Scientific), graphite felt (Fuel Cell Store).

### Preparation of BiOCl coated electrodes

The graphite felt from Fuel cell store was treated before use by immersing it in 1 M HNO<sub>3</sub> for 24 hours, washed with deionized water and isopropanol and then dried at 100 °C in an oven. BiOCl and conductive carbon are mixed using a mortar pestle. The electrode slurry for the coated BiOCl electrode is prepared by mixing BiOCl, conductive carbon and Nafion® in the weight percentages of 70%, 15% and 15% respectively along with an adequate amounts of water and isopropanol. The slurry is coated on graphite felt using an air brush.

### Preparation of the BiOCl and VOSO<sub>4</sub> silica gel

The VOSO<sub>4</sub> containing gel is prepared by mixing 15% (weight/volume %) of fumed silica with VOSO<sub>4</sub> dissolved in an acid mixture of 1 M HCl + 1 M H<sub>2</sub>SO<sub>4</sub>. The fumed silica is added gradually with continuous stirring and the resulting solution is left overnight to get a vanadium containing silica gel. A similar method is followed to prepare the electrolyte gel with 1 M HCl + 1 M H<sub>2</sub>SO<sub>4</sub>. For the BiOCl, the cell was tested with both BiOCl electrode coated on graphite felt as well as BiOCl containing silica gel. The BiOCl containing silica gel was prepared in a way similar to VOSO<sub>4</sub> containing silica gel. In the BiOCl coated electrode configuration, an acid mixture of 1 M HCl + 1 M H<sub>2</sub>SO<sub>4</sub> is used as electrolyte. Cells were assembled by stacking layers of vanadium and electrolyte gels and immersing BiOCl electrode in liquid electrolyte.

### Electrochemical screening

The electrochemical methods used were cyclic voltammetry (CV), electrochemical impedance spectroscopy (EIS), and galvanostatic charge discharge (GCD). Biologic VSP-300, electrochemical test station was used for all the electrochemical measurements. The 0.5 cm × 0.5 cm BiOCl coated graphite felt electrodes connected with titanium wires were used as working electrodes (WE); The 0.5 × 0.5 cm platinum foils obtained from Thermo-Fisher Scientific were used as counter electrodes (CE). These Pt foils were cleaned with 1 M HNO<sub>3</sub> solution. The Ag/AgCl (sat. KCl) reference electrodes

(RE) were obtained from CH Instruments. A 0.5 cm × 0.5 cm graphite felt pieces were used as working electrodes for the cyclic voltammetry analysis of gel type electrodes. For the ionic conductivity measurement via EIS, a custom cell was assembled by fixing two parallel, identical pieces of Pt foils 0.2 cm apart. The cell was monthly calibrated by a 1 M KCl solution at room temperature and cleansed with HNO<sub>3</sub> solutions. The cell constant value after calibration is 0.7895 cm<sup>-1</sup>.

### XRD measurement

XRD measurements were performed on the Bruker D8 Advance diffractometer operating in the reflection mode with Cu-Kα radiations and diffracted beam monochromator, using a step scan mode with the step size of 0.02° (2θ) and 2 s time per step.

### Scanning electron microscopy (SEM)

The morphology of the BiOCl coated electrode was studied by scanning electron microscopy (SEM) using a ThermoFisher Scientific Phenom G6 Pro operated at an accelerating voltage of 15 kV.

### Acknowledgements

This research was undertaken thanks in part to funding from the Canada First Research Excellence Fund and the NSERC I2I fund.

### Conflict of Interests

The authors declare no conflict of interest.

### Data Availability Statement

The data that support the findings of this study are available from the corresponding author upon reasonable request.

**Keywords:** battery materials · energy storage · gels · vanadium

- [1] S. Chu, A. Majumdar, *Nature* **2012**, *488*, 294–303.
- [2] W. Wang, B. Yuan, Q. Sun, R. Wennersten, *J. Energy Storage* **2022**, *52*, 104812.
- [3] P. Lyu, X. Liu, J. Qu, J. Zhao, Y. Huo, Z. Qu, Z. Rao, *Energy Storage Mater.* **2020**, *31*, 195–220.
- [4] a) K. Mongird, V. V. Viswanathan, P. J. Balducci, M. J. E. Alam, V. Fotedar, V. S. Koritarov, B. Hadjerioua, Pacific Northwest National Lab.(PNNL), Richland, WA (United States), **2019**; b) J. Balaji, M. G. Sethuraman, S.-H. Roh, H.-Y. Jung, *Polym. Test.* **2020**, *89*, 106567.
- [5] Q. Huang, Q. Wang, *ChemPlusChem* **2015**, *80*, 312–322.
- [6] a) S. V. Venkatesan, K. Karan, S. R. Larter, V. Thangadurai, *Sustain. Energy Fuels* **2020**, *4*, 2149–2152; b) S. Hou, L. Chen, X. Fan, X. Fan, X. Ji, B. Wang, C. Cui, J. Chen, C. Yang, W. Wang, C. Li, C. Wang, *Nat. Commun.* **2022**, *13*, 1281; c) P. Navalpotro, J. Palma, M. Anderson, R. Marcilla, *Angew. Chem.* **2017**, *129*, 12634–12639; d) E. Ventosa, *Curr. Opin. Chem. Eng.* **2022**, *37*, 100834.
- [7] M. Skyllas-Kazacos, A. Banzato (Unisearch Limited), WO 02/11227 Al, **2002**.
- [8] G. Yadav, J. Huang, S. Banerjee (Urban Electric Power Inc.), WO 2021/081394 Al, **2021**.
- [9] a) C. Y. Yang, J. Chen, T. T. Qing, X. L. Fan, W. Sun, A. von Cresce, M. S. Ding, O. Borodin, J. Vatamanu, M. A. Schroeder, N. Eidson, C. S. Wang, K. Xu, *Joule* **2017**, *1*, 122–132; b) L. Suo, O. Borodin, W. Sun, X. Fan, C. Yang, F. Wang, T. Gao, Z. Ma, M. Schroeder, A. von Cresce, S. M. Russell, M. Armand, A. Angell, K. Xu, C. Wang, *Angew. Chem.* **2016**, *128*, 7252–7257.
- [10] W.-Y. A. Lam, K.-Y. Chan, C.-Y. V. Li, *J. Electrochem. Soc.* **2023**, *169*, 120538.
- [11] a) D.-H. Nam, M. A. Lumley, K.-S. Choi, *Chem. Mater.* **2019**, *31*, 1460–1468; b) F. Chen, Y. Huang, L. Guo, L. Sun, Y. Wang, H. Y. Yang, *Energy Environ. Sci.* **2017**, *10*, 2081–2089; c) D.-H. Nam, K.-S. Choi, *ACS Sustainable Chem. Eng.* **2018**, *6*, 15455–15462; d) J. Chang, F. Duan, C. Su, Y. Li, H. Cao, *Environ. Sci.: Water Res. Technol.* **2020**, *6*, 373–382.
- [12] D.-H. Nam, K.-S. Choi, *J. Am. Chem. Soc.* **2017**, *139*, 11055–11063.
- [13] M. Skyllas-Kazacos, M. Kazacos, *J. Power Sources* **2011**, *196*, 8822–8827.
- [14] H. Wang, S. Y. Sayed, E. J. Luber, B. C. Olsen, S. M. Shirurkar, S. Venkatakrishnan, U. M. Tefashe, A. K. Farquhar, E. S. Smotkin, R. L. McCreery, J. M. Buriak, *ACS Nano* **2020**, *14*, 2575–2584.
- [15] W. Wang, X. Fan, J. Liu, C. Yan, C. Zeng, *RSC Adv.* **2014**, *4*, 32405–32411.

---

Manuscript received: October 4, 2023

Revised manuscript received: November 30, 2023

Accepted manuscript online: December 5, 2023

Version of record online: December 15, 2023

---